JACS
JOURNAL OF THE AMERICAN CHEMICAL SOCIETY
Article
pubs.acs.org/JACS

DNA Origami Directed Au Nanostar Dimers for Single-Molecule Surface-Enhanced Raman Scattering

Swati Tanwar,[†] Krishna Kanta Haldar,[‡] and Tapasi Sen*[,†]

[†]Institute of Nano Science and Technology, Phase-10, Sector-64, Mohali, Punjab-160062, India

[‡]Department of Chemical Sciences, School of Basic and Applied Sciences, Central University of Punjab, Bathinda, Punjab-151001, India

Supporting Information

ABSTRACT: We demonstrate the synthesis of Au nanostar dimers with tunable interparticle gap and controlled stoichiometry assembled on DNA origami. Au nanostars with uniform and sharp tips were immobilized on rectangular DNA origami dimerized structures to create nanoantennas containing monomeric and dimeric Au nanostars. Single Texas red (TR) dye was specifically attached in the junction of the dimerized origami to act as a Raman reporter molecule. The SERS enhancement factors of single TR dye molecules located in the conjunction region in dimer structures having interparticle gaps of 7 and 13 nm are 2×10^{10} and 8×10^{9}, respectively, which are strong enough for single analyte detection. The highly enhanced electromagnetic field generated by the plasmon coupling between sharp tips and cores of two Au nanostars in the wide conjunction region allows the accommodation and specific detection of large biomolecules. Such DNA-directed assembled nanoantennas with controlled interparticle separation distance and stoichiometry, and well-defined geometry, can be used as excellent substrates in single-molecule SERS spectroscopy and will have potential applications as a reproducible platform in single-molecule sensing.

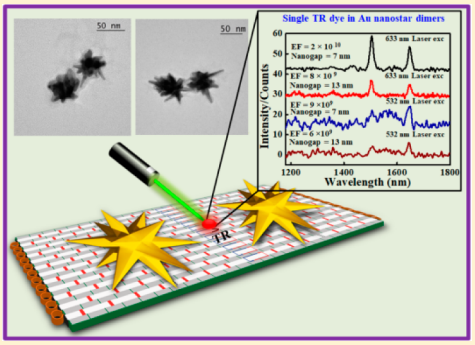

INTRODUCTION

DNA origami offers a novel nanostructure with features of precise addressability and defined size and shapes for the creation of various functional structures and their applications in single-molecule analyses.[1,2] Since the first report of the DNA origami method by Paul Rothemund, this versatile technique has been utilized extensively for precise arrangement of nanoparticles of arbitrary size at a predefined interparticle distance with sub-nm accuracy, controlled spatial orientation, and tunable stoichiometry.[3,4] DNA origami-assembled plasmonic nanostructures such as dimeric nanostructures are found to be promising for single-molecule spectroscopic techniques like surface-enhanced fluorescence and Raman signal enhancement.[5−7] Surface-enhanced Raman spectroscopy (SERS) is a powerful vibrational spectroscopy technique that allows for highly sensitive structural detection of low concentration analyte molecule as vibrational fingerprint of each molecule is unique.[8,9] The SERS technique has been employed in various applications including biological and chemical sensing and ultrasensitive detection of explosives and in food safety by using plasmonic nanoparticles as SERS substrates.[10−12] Owing to the electromagnetic field enhancement associated with "hotspots" of plasmonic nanostructures, extremely low intrinsic Raman cross section of molecules is dramatically increased, hence enabling their detection down to single-molecule level.[13−15] In light of these fascinating properties of plasmonic nanoantennas, many examples have been shown in the past highlighting their potential uses as optical sensors and photonic devices and in imaging and single-molecule spectroscopy applications.[5,16−18] Au nanostructures are of particular interest because of their stability, nontoxicity, and easy bioconjugation ability.[19] Kühler et al. reported the synthesis of Au nanoparticle dimers prepared by DNA origami and their use as efficient SERS substrate.[20] Such a DNA origami-based nanoantenna with tunable nanogap provides sequence-defined binding sites to place analyte molecules of interest specifically in the hotspot region, and this unique feature marks a clear advantage compared to other methods that rely on random adsorption of molecules to the nanoantenna gap.[20]

Such fabrication processes are also much more cost-effective than widely used top-down lithographic techniques to create nanoantenna materials.[21] Current approaches to fabricate nanoantennas via self-assembly or wet chemical synthesis do not achieve the required structural control and cannot provide docking sites in the hotspot for placing biomolecules of interest in the hotspot.[5] The effectiveness of SERS-active structures generally depends on the geometry of the nanoparticle, type of material, and interparticle distance. Spherical Au and Ag nanoparticles along with core−shell and anisotropic nanostructures have been extensively used from long time as SERS substrates because of their easy tunable plasmon wavelength,

Received: September 29, 2017
Published: November 13, 2017

DOI: 10.1021/jacs.7b10410
J. Am. Chem. Soc. 2017, 139, 17639−17648

which on matching with excitation wavelength results in ultrahigh sensitivity with detection limits in the low femtomolar or even attomolar range.[22−27] Apart from using ultralow analyte concentrations different strategies have been adopted aiming at the detection of single molecules based on SERS.[7,28,29] For example, Prinz et al. demonstrated SERS from AuNP dimer on DNA origami substrates for the identification of specific Raman bands of single TAMRA molecules attached to the DNA origami.[30] The sensitivity of single-molecule SERS was further enhanced by an additional Ag layer grown on the AuNPs dimer on triangular DNA origami for single TAMRA and Cy3 molecule placed in the hotspot because of the increase of the electromagnetic field enhancement due to Ag shell.[21] Very recently, SERS activities of single Au nanolenses with three different geometrical arrangements have been assessed.[31] In another study, Prinz et al. presented the interaction of Au NP dimers with graphene assembled on DNA origami nanostructures which yields higher SERS activity for the hybrid structure compared to their individual entities.[32]

Among all the anisotropic shapes, gold nanostars are especially attractive due to their particular structural and optical properties, including strong localized plasmonic fields at their sharp edged tips, and tunable NIR resonances for their use in sensing, SERS, biological imaging, and biomedical applications.[27,33−37] The strong electromagnetic field generated at the sharp tips of gold nanostars can lead to an extraordinary field enhancement[38−41] and also the plasmons focused at the core couples with the tips in gold nanostar structures,[23] making it an outstanding candidate for numerous spectroscopic applications. It has been demonstrated that gold nanostars with sharp tips gives much higher electric field enhancement and thus excellent SERS efficiency compared to spherical or rod shaped gold nanoparticles under similar experimental conditions.[27,34] The electromagnetic field in the vicinity of Au nanostars' tips can be enhanced by several orders of magnitude by simply tuning the sharpness and number of tips which further results in creation of lots of "hotspots" required for highly significant SERS enhancement.[38] The Liz-Marzán group extensively studied experimentally the SERS activities of gold nanostars for numerous applications[42] such as in food safety for detection of pesticides in apples.[34] Haes et al. used functionalized Au nanostar as SERS-based detection of uranyl and emphasized that the tip architecture plays a key role in determining SERS intensities.[43] Abajo et al. very recently provided in-depth insight for understanding and designing optimized SERS substrate based on anisotropic Au nanoparticles using computation techniques.[44] Aizpurua et al. demonstrated the optical response of plasmonic nanogaps with narrow junctions by employing Quantum Corrected Model that allows accounting for the quantum tunneling with fully classical simulations.[45] The optical properties of multiscale plasmonic dimers with two or more length scales (fine, medium, coarse) and their applications in SERS spectroscopy have been described by Odom et al.[46] Vo-Dinh et al.[33] measured the SERS enhancement factor of 52 nm sized Au nanostars which was found to be 5×10^3 for p-MBA molecule. Fabris et al. employed Au nanostars for ultrasensitive detection of 4-mercaptobenzoic acid in femtomolar regime with SERS enhancement factor of 10^9.[47] It has been reported that the SERS enhancement factor is strongly dependent on the geometry of the nanostructure as well as the number of hotspots compared to isolated particles and strongly increases with decreasing the interparticle gap.

So far most of the previous efforts focused on the immobilization of spherical Au nanoparticles and Au nanorods on DNA origami. To the best of our knowledge, there is no report in literature to date on formation of Au nanostar dimer by using DNA origami template. The present report is the first study on the synthesis of Au nanostar dimer structures with tunable interparticle gap and controlled stoichiometry and their use as an excellent SERS substrate for single-molecule detection. Single-molecule SERS is useful for exploration of subtle spectroscopic phenomena such as isotopic substitutions in single molecules, true homogeneous broadening of Raman peaks and Raman excitation profiles of individual molecules that are difficult to study via ensemble approach.

Here, we report the design of Au nanostar dimer assembled on DNA origami nanostructure with precisely tunable interparticle gap. Au nanostars with uniform and sharp tips were immobilized on rectangular DNA origami dimerized structures to form dimeric Au nanostars. Single Texas red (TR) dye, which acts as a Raman reporter molecule, was incorporated within the origami structure in between two Au nanostars in the conjunction region that is present between tips and cores of two nanostars. It was found that the SERS enhancement factor of single TR dye placed in the center of nanogap of Au nanostar dimer structure is 2×10^{10} which is unprecedented for such dye. Such high value of enhancement factor ensures the specific detection of single analyte molecule. Such hybrid nanoantenna materials assembled on DNA origami substrates with controlled nanogap and stoichiometry will have potential applications as a cost-effective and reproducible platform for single-molecule sensing.

EXPERIMENTAL SECTION

Materials. Gold chloride trihydrate ($HAuCl_4 \cdot 3H_2O$), trisodium citrate, L-ascorbic acid, silver nitrate, ethylenediaminetetraacetic acid disodium salt (EDTA), Trizma base, tris(carboxyethyl)phosphine hydrochloride (TCEP), and sodium chloride (NaCl) were purchased from Sigma-Aldrich and $MgCl_2$ from SRL. M13mp18 single-stranded DNA was procured from New England Biolabs and was used without further treatment. All unmodified staple strands were purchased from Integrated DNA Technologies, Inc. (IDT) in unpurified form (standard desalting). 5′-Thiol-modified single-stranded DNA was purchased from IDT after HPLC purification. All of these reagents were used without further purification. Amicon filters with 0.5 mL centrifugal volume, 100 kDa molecular weight were purchased from Sigma-Aldrich. Freeze N Squeeze spin columns were purchased from Bio-Rad. Milli-Q (MQ) water was used for all the experiments.

Buffers. DNA origami samples were annealed in 1× TAE buffer (40 mM Tris, 20 mM acetic acid, 1 mM EDTA) containing 12.5 mM magnesium chloride, pH 8.0.

Synthesis of DNA Origami. The rectangular DNA origami structure was synthesized by following the method described by Rothemund.[1] M13mp18 single-stranded DNA was used as the scaffold. Briefly, the rectangular DNA origami was self-assembled using a long single-stranded M13mp18 viral genomic DNA folded by a set of ∼200 short staple strands using a 1.5 h annealing program. Annealing was performed in 1× TAE buffer with scaffold concentration of 2 nM, 10-fold excess of regular staples, and 20-fold excess of modified staples.

Purification of Rectangular DNA Origami Monomer. Annealed DNA origami monomer was purified using Amicon filter (100 kDa) that was filled with 50 μL of PCR mixture and 450 μL of 1× TAE buffer (pH 8) with 12.5 mM $MgCl_2$ and spun at 14000*g* for 5 min at 4° C. This was followed by three times washing with 500 μL of 1× TAE, 12.5 mM $MgCl_2$ buffer. Finally an Amicon filter was inverted in a fresh micro centrifuge tube and spun at 5000*g* for 10 min to collect purified origami.

DOI: 10.1021/jacs.7b10410
J. Am. Chem. Soc. 2017, 139, 17639−17648

Dimerization of Rectangular DNA Origami. Dimerization of rectangular DNA origami was done according to previously reported protocol.[48] To an equimolar mixture of unpurified origami A and origami B solution, 24 branching staples were added in 40-fold excess and the mixture was incubated at room temperature for 24 h in 50× TAE with 12.5 mM $MgCl_2$. The edges of each origami monomer were extended with 24 T-loop edge staples of various lengths in the opposite side of the junction to restrict the uncontrolled polymerization into ribbons of nonuniform lengths (shown in Scheme 1).[49]

Scheme 1. Schematic Design of Au Nanostar Dimers on Dimerized Rectangular Origami Structures

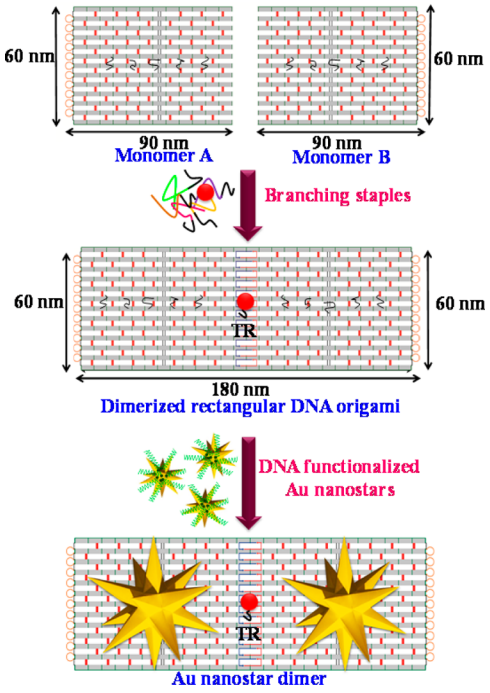

Purification of DNA Origami Dimer. Dimerized rectangular DNA origami was purified using Sephacryl S-300 HR resin. Polypropylene columns were hand packed with 750 μL of liquid resin and then spun at 1400 g at 10 °C for 2 min. The column was further washed with 500 μL of 1× TAE buffer (pH 8) with 11 mM $MgCl_2$ and spun at 1400*g* for 2 min. This procedure was repeated thrice to completely equilibrate the column. After addition of dimerized rectangular DNA origami solution, column was spun at 1400*g* for 5 min at 10°C. Collected purified origami was used for Atomic force microscopy (AFM) and transmission electron microscopy (TEM) imaging and also for immobilization of DNA-functionalized Au nanostars.

The monomer and dimerized rectangular DNA origami structures were also purified using gel electrophoresis. For gel electrophoresis, 1% agarose in 1× TAE buffer was heated to boiling and cooled to 50 °C followed by addition of 1 M $MgCl_2$ (final concentration of 12.5 mM $MgCl_2$) to provide stability to DNA origami nanostructures during the run. Staining was done using ethidium bromide. Gel lanes were filled with 25 μL of unpurified dimerized DNA origami and 5 μL of loading buffer. For running the gel a voltage of 70 V was applied for 2 h. Gel assembly was kept in ice bath during 2 h of run time to prevent denaturation of DNA origami because of heat. After running the gel, the bands were visualized and imaged using ChemiDoc XRS+ molecular imager with image lab software and extracted using Freeze N Squeeze spin columns.

Incorporation of Single Texas Red Dye in DNA Origami. Texas red (TR) is a red fluorescent dye that is extensively used for staining cell specimens in biology and also in single-molecule fluorescence resonance energy transfer studies.[50,51] For the incorporation of single TR dye molecule in the center of the dimerized rectangular DNA origami, we have modified one branching staple by attaching with a TR moiety at the 3′ end. Usual unmodified branching staple was replaced by the dye modified staple during dimerization step. The rest of the dimerization conditions and concentrations were similar to those for the above-mentioned protocol.

Preparation of Au Nanostars. Au nanostars were synthesized using previously reported method after slight modifications.[52] Au nanostars were prepared based on a seed-mediated growth method. At first, citrate stabilized Au nanoparticles seed solution was synthesized by following a well-known citrate reduction method.[53] Briefly, to a 12.5 mL boiling solution of 1 mM $HAuCl_4$, 2 mL of 1.5% trisodium citrate was added under vigorous stirring. The color of the solution changes from light yellow to red due to the formation of Au nanoparticles within 5−10 min. The solution was stirred continuously with heating for another 20 min. Finally, the solution was cooled to room temperature under stirring.

Au nanostars were prepared by adding 150 μL of the above-synthesized seed solution to growth solution containing 10 mL of 0.15 mM $HAuCl_4$ with 10 μL of 1 M HCl under mild stirring. It was followed by simultaneous addition of 40 μL of 0.01 M $AgNO_3$, 50 μL of 0.01 M ascorbic acid, and 20 μL of 0.01 M SDS solution, respectively. To halt the process of nucleation, the Au nanostar solution was immediately given one centrifugal wash at 4000*g* for 15 min, followed by resuspension in water (MQ). Seed solutions were ultrasonicated for 10 min before addition to growth solution at a frequency of 53 kHz.

Functionalization of Au Nanostars with DNA Oligonucleotides. The thiolated DNA oligonucleotides were reduced by incubating them with 0.2 M TCEP (1:200 molar ratio of DNA:TCEP) in water (MQ) for 3 h. The DNA functionalization of Au nanostars was performed by following the method reported by Mirkin et al.[54] with the following DNA sequence containing a thiol modification at the 5′ end: 5′-thiol-CGTCGTATTCGATAGCTTAG-3′. The DNA-functionalized Au nanostars were washed using 100 kDa Amicon filter to remove excess unbound oligonucleotides and were finally resuspended in 0.5× TAE-Mg^{2+} buffer.

Hybridization between Au Nanostars and DNA Origami. The dimerized DNA origami was mixed with DNA-functionalized Au nanostars at a molar ratio of 1:1 in 0.5× TAE Mg^{2+} with 0.3 M NaCl. The mixture was heated repeatedly between 40 and 20°C for 12 h, being kept in a PCR thermocycler. The final product was used for TEM imaging and Raman measurements.

UV−Visible and Steady-State Photoluminescence Spectroscopy. UV−visible absorption spectra of Au nanoparticles and nanostars were recorded at room temperature with a Shimadzu UV-2600 spectrophotometer. Emission spectra of TR dye were measured at room temperature using a FS5 steady state fluorescence spectrometer from Edinburg Instruments.

Transmission Electron Microscopy (TEM). Structural characterization of DNA origami and Au nanostars were performed by recording TEM images using a JEOL 2100 microscope with a lanthanum hexaboride (LaB_6) filament at accelerating voltages of 120 and 200 kV, respectively. Average nanoparticle size was measured using Gatan microscopy suite software. For recording images, purified DNA origami (6 μL) was dropped onto a TEM grid (pre-activated using 1 M $MgCl_2$) for 10 min followed by washing with water (MQ). Negative staining of origami was done using (2% w/v) uranyl acetate for 2 min.

Atomic Force Microscopy (AFM). AFM imaging of DNA origami samples were done on mica sheets of V1 quality using dry AFM. Bruker Multimode 8 scanning probe microscope with silicon cantilever (Bruker) was used for AFM imaging in tapping mode analysis. At first, mica sheet was fixed on round metal plate (Dia-1.5 mm) using transparent nail polish and freshly cleaved 5−6 times. It was then incubated with 50 μM $MgCl_2$ solution for 5 min followed by washing 3−4 times with H_2O. After drying the substrate in air, 10 μL of purified origami was placed on mica substrate for 10 min, followed by washing with water and drying using a gentle breeze of N_2.

DOI: 10.1021/jacs.7b10410
J. Am. Chem. Soc. 2017, 139, 17639−17648

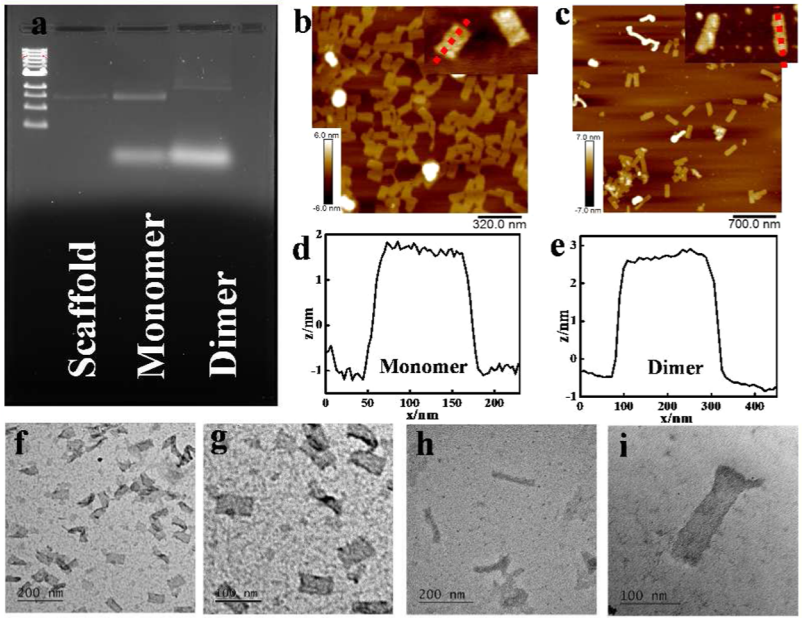

Figure 1. Gel electrophoresis images of rectangular DNA origami monomer and dimer (a). AFM images of origami monomer and dimer, respectively (b,c) and corresponding height profiles (d,e). TEM images of origami monomer (f,g) and origami dimer (h,i).

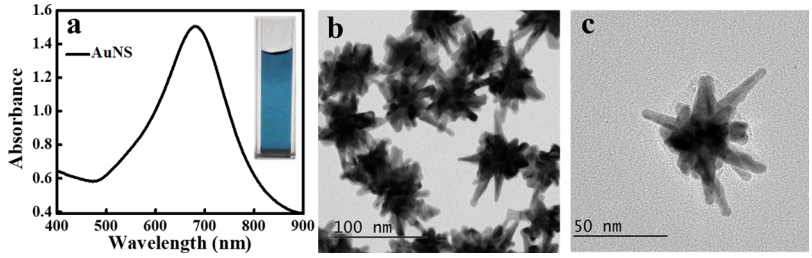

Figure 2. (a) UV−vis spectrum of Au nanostars (inset: photograph of as-prepared Au nanostar solution). (b,c) TEM images of Au nanostars.

Immobilization of Au nanostars on Si wafer for AFM correlated Raman measurements. Si wafer pieces (1 × 1 cm^2 size) were oxygen plasma cleaned (using Plasma bonder from Omicron scientific equipment Co.) for 5 min to ensure hydrophilicity of the wafer surface. The wafers were then washed twice with 1:1 solution of ethanol and distilled water followed by incubation with dilute solution of Au nanostars−DNA origami structure in 10× TAE with 200 mM $MgCl_2$ for 20 min. This was followed by washing with MQ and drying with gentle breeze of N_2 to ensure uniform and complete coverage of surface.

Raman Measurements and Calculation of the Enhancement Factor (EF). Surface-enhanced Raman scattering (SERS) spectra were acquired with a confocal Raman microscope (Witec alpha 300 R) equipped with an upright optical microscope (Zeiss). The measurements were performed in air using laser light at 532 and 633 nm lasers using 100 × objective (NA = 0.9) to a diffraction-limited spot of about 1 μm^2 on Si wafer. The laser power was set to 1 mW with integration time 4 s (for TR dye bound to Au nanostar-DNA origami structures) or 10 s for TR bound to DNA origami structures and bulk dye. Reference Raman measurements of the TR were performed with bulk solution at 1.5 mM concentration. AFM correlated Raman measurements were performed by introducing a prominent feature (a scratch in Si wafer samples) and scanning almost the same area by AFM imaging and confocal Raman microscopy and then overlapping the images by manually relocating the pronounced feature in both images. The SERS enhancement factor was calculated using eq 1.[24,25,55,56]

$$EF = \frac{N_{bulk}}{N_{SERS}} \frac{I_{SERS}}{I_{bulk}} \quad (1)$$

where I_{SERS} and I_{bulk} are the intensities of the vibrational peaks in SERS and normal Raman measurements using bulk dye solution, respectively, and N_{bulk} and N_{SERS} are the number of molecules contributing to Raman signal in normal Raman measurement using bulk dye and the SERS measurements using TR dye bound to Au nanostar−DNA origami structures, respectively. This was determined by counting the number of Au nanostar−DNA origami structures in the confocal area using AFM correlated Raman images. I_{SERS} was taken from the strongest Raman peak of TR dye. SERS peak at 1647 cm^{-1} for 532 nm laser excitation and peak at 1504 cm^{-1} in case of 633 nm laser excitation were used for calculating EF.[24,50] I_{bulk} represents Raman intensity at 1647 cm^{-1} peak for 532 nm laser and 1504 cm^{-1} for 633 nm laser from TR bulk solution at 1.5 mM concentration.

RESULTS AND DISCUSSION

Characterization of DNA Origami. For the synthesis of Au nanostar dimer on DNA origami, two rectangular origami have been linked together to form dimerized rectangular DNA origami (presented in Scheme 1). After the formation of monomer and dimerized rectangular DNA origami, the structures were characterized by agarose gel electrophoresis. Gel images shown in Figure 1a indicates the formation of monomer and dimerized rectangular DNA origami. AFM and TEM studies further reveal the formation of a high yield of DNA origami monomer (>95%) and dimer structures. Figure 1b shows the AFM images of rectangular DNA origami monomer of dimension of ∼90 × 60 nm, which can hold only a large Au nanostar. AFM images shown in Figure 1c reveals the

DOI: 10.1021/jacs.7b10410
J. Am. Chem. Soc. 2017, 139, 17639−17648

formation of dimerized rectangular DNA origami with a dimension of ~180 × 60 nm that is capable of holding two Au nanostars. Height profiles of rectangular DNA origami monomer and dimer structures are represented in Figure 1d, e. TEM images of origami monomer and dimer as shown in Figure 1f–i confirm the formation of rectangular origami of dimension of ~90 × 60 nm and ~180 × 60 nm, respectively, which is in consistent with previous study.[48] For immobilization of DNA-functionalized Au nanostars on DNA origami, five staples of each origami monomer were extended at the 3′ end enabling immobilization of one Au nanostar on each monomer as represented in Scheme 1.

UV–Vis and TEM Studies. Figure 2a shows the UV–visible spectrum of as synthesized Au nanostars using seed mediated method in aqueous medium without any surfactant.[52] The presence of longitudinal surface plasmon resonance (LSPR) band at 680 nm (Figure 2a) along with a very weak hump at 520 nm indicates the formation of anisotropic Au nanostructures with very sharp tips. Further identification of these structures with transmission electron microscopy (TEM) confirms the formation of Au nanostars with sharp tips uniformly distributed over the core (~10–15 tips) having radius of curvature of 2–3 nm (clearly shown in Figure 2b). Average size of Au nanostars was found to be 70 ± 5 nm (TEM image shown in Figure 2c). Such Au nanostars with sharp and uniform tips giving LSPR centered at 680 nm can strongly couple with a red-emitting dye like TR and are expected to give highly enhanced SERS signal.

Characterization of DNA-Functionalized Au Nanostars. Aqueous medium synthesis of Au nanostructures without using any surfactant enables efficient functionalization and excludes the step of repeated washing required prior DNA functionalization to remove excess surfactant. DNA functionalization of as synthesized Au nanostars was carried out using a well-established protocol of salt aging.[54] The density of DNA oligonucleotides on surface of Au nanoparticles depends on the final concentration of NaCl that can reduce the phosphate backbone repulsion between oligonucleotides. Thus, to achieve uniform and dense DNA coating on Au nanostar surface, the concentration of NaCl was increased slowly from 0 to 750 mM during the functionalization step (Figure 3a). UV–vis absorption spectra show no significant change in the position of LSPR band of Au nanostars after DNA functionalization (Figure 3b), suggesting no morphological changes after DNA modification. These DNA-functionalized Au nanostars were also found to be stable in high salt concentration of 500 mM NaCl (shown in Figure 3c), which reveals their stability in high salt concentration that is required for the immobilization of Au nanostars on DNA origami.

Photoluminescence Study. To ensure the successful incorporation of a single TR dye molecule in the center of the DNA origami dimer (shown in Scheme 1), PL spectra of the dye-bound DNA origami dimer were recorded after purification with Sephacryl S-300 resin to remove excess unbound dye-labeled staple strands. The emission spectrum of the dye centers at 614 nm upon excitation with 594 nm (shown in Figure S1), which suggests the incorporation of dye inside the origami.

Assembly of Au Nanostars on Dimerized Origami with Tunable Nanogap. The procedure of coupling two Au nanostars on dimerized rectangular origami is schematically shown in Scheme 1. A set of five staples of each origami monomer unit were extended at the 3′ end in order to bind

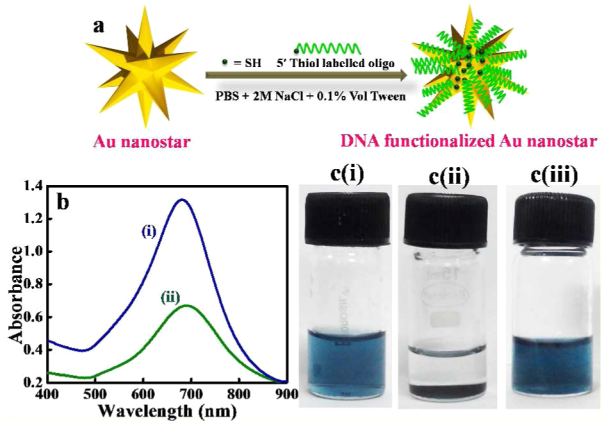

Figure 3. (a) Schematic representation of DNA functionalization of Au nanostars. (b) UV–visible spectra of Au nanostars before (curve (i)) and after DNA functionalization (curve (ii)). (c) Photographs of Au nanostars solution without salt (i), Au nanostars solution without DNA functionalization with PBS–500 mM NaCl buffer (ii), and DNA-functionalized Au nanostars solution with PBS–500 mM NaCl (iii).

complimentarily to the thiolated oligonucleotides that were coated on the surface of Au nanostars. In this way, after annealing together each monomer origami can bind to a single Au nanostar specifically through the hybridization interactions between complementary oligonucleotides, overall resulting dimer of Au nanostars on dimeric origami (presented in Scheme 1). In order to achieve tunable interparticle gap, five capturing strands were chosen from different positions of the origami monomer and extended at the 3′ end. Au nanostar dimers with two different average gaps were synthesized for understanding the effect of interparticle gap on SERS efficiency shown in Scheme S1. AFM imaging (shown in Figure 4a,b)

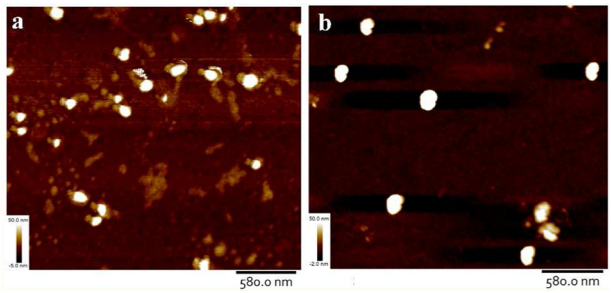

Figure 4. AFM images of (a) Au nanostar monomer on DNA origami and (b) Au nanostar dimer on DNA origami.

confirms the formation of Au nanostar monomer and dimer structures on DNA origami. In case of Au nanostar monomer (Figure 4a), DNA origami template is clearly visible. However, in case of Au nanostar dimer (Figure 4b) DNA origami template probably got hidden behind the Au nanostar dimer.

From TEM measurements of the dimer samples (shown in Figure 5), average gaps of 13 ± 1 and 7 ± 1 nm (Au nanostar core to core) were obtained. We have also calculated the tip-to-tip distances(d) in the conjunction region that is present between tips and cores of two nanostars after considering several TEM images of nanostar dimer structures. The tip-to-tip distances were found to lie in the ranges of ~1 nm ≤ d ≤ 4 nm and ~2 nm ≤ d ≤ 4.8 nm for 7 and 13 nm nanogap dimer structures, respectively. For getting an average interparticle gap

DOI: 10.1021/jacs.7b10410
J. Am. Chem. Soc. 2017, 139, 17639–17648

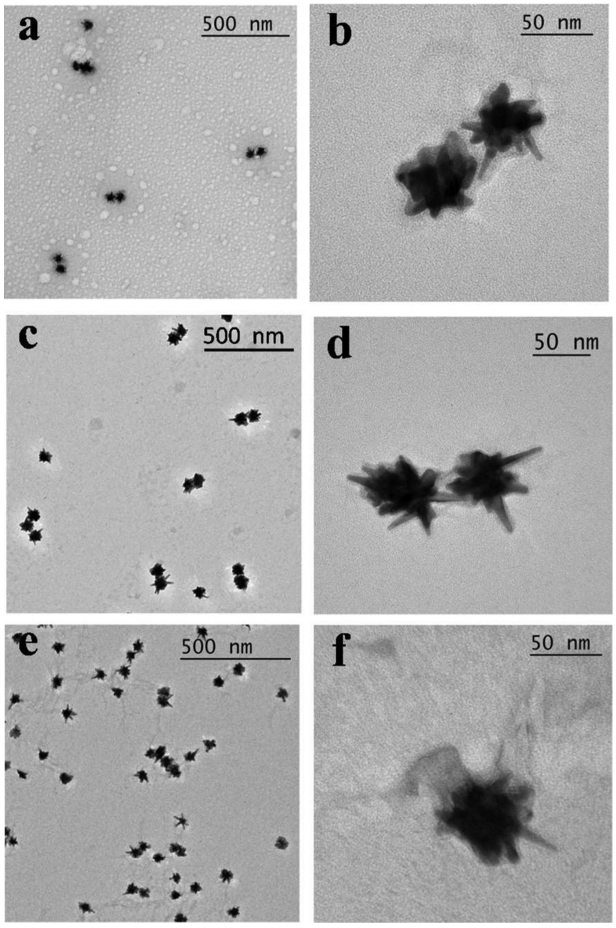

Figure 5. (a–d) TEM images of Au nanostar dimers on DNA origami with different interparticle gaps: (a,b) average interparticle gap of 13 nm and (c,d) gap of 7 nm. (e,f) TEM images of Au nanostar monomer on DNA origami.

of ~7 nm, capturing staple strands were taken at the position of 82,83,111,85,86 of one monomer (monomer A) and 81,82, 83,111,85 of another monomer (monomer B). Similarly, for average gap of 13 nm, capturing staples used were 81,82,83,111,85 and 82,83,111,85,86 for monomers A and B, respectively. A schematic sketch of rectangular DNA origami design showing positions of capturing staples and dye labeled staple is presented in Scheme S1.

To further investigate the influence of Au nanostar stoichiometry on the electromagnetic field enhancement in the hotspot, monomer Au nanostars bound to dimerized origami were also prepared along with Au nanostar dimer bound to origami by removing capture strands from one monomer unit. It can be emphasized that further reduction in the interparticle gap is possible by changing the capturing strands position (83,111,85,86,87 for monomer A and 80,81,82,83,111 for monomer B) on the origami. However, it was found from TEM study of such Au nanostar dimer structures that the tips are touching to each other in the conjunction region between two nanostars and core-to-core distance between two nanostars becomes ~4 nm (shown in Figure S2a). Raman measurement of this dimer structure showed no enhancement of Raman signal of TR dye molecule and even the characteristic peaks were also not visible in the SERS spectrum as presented in Figure S2. This may be due to quantum tunneling that takes place for very narrow gaps ($d \leq$ 0.3–0.4 nm) and results in strong reduction in the electromagnetic field enhancement as described by Aizpurua et al.[45] In this case, there is no gap between tips of two particles in the conjunction region which leads to quantum tunnelling and results in no enhancement of Raman signal of TR which is placed in between two nanostars in the conjunction region. In a recent theoretical study, Abajo et al. also mentioned that the SERS signal enhancement can be quenched when tips and valleys are closely intertwined.[44]

AFM Correlated Single-Molecule Raman Measurement. The assembled Au nanostars dimer on DNA origami with various nanogaps were investigated for its potential to be

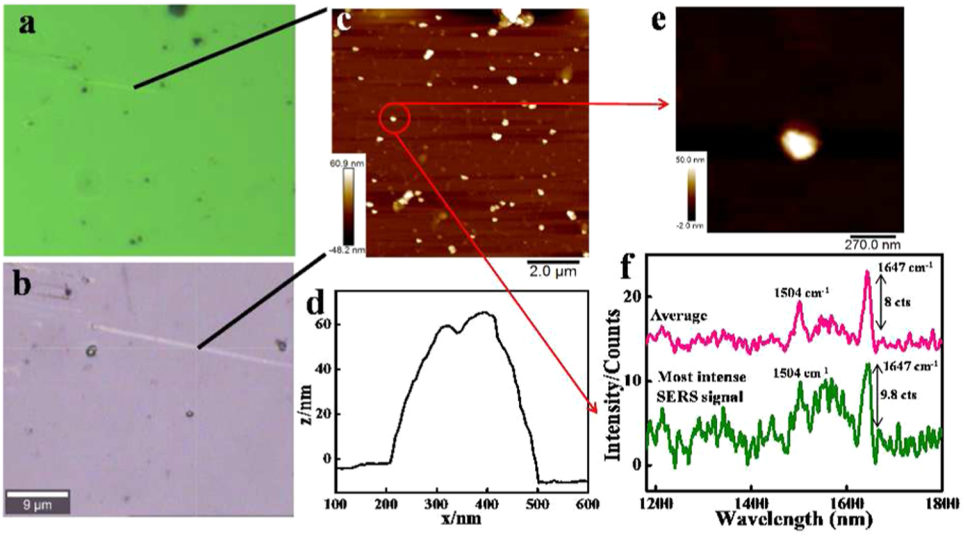

Figure 6. AFM-correlated Raman measurements using 532 nm laser source. (a) Optical image taken using 10× objective of AFM. (b) Optical image taken using 100× objective of confocal Raman microscope. (c) AFM images of Au nanostar dimer with gap of 7 nm and (d) corresponding height profile. (e) AFM image of single Au nanostar dimer nanostructure. (f) Average and most intense SERS spectra of TR dye bound to Au nanostar dimer on DNA origami.

DOI: 10.1021/jacs.7b10410
J. Am. Chem. Soc. 2017, 139, 17639–17648

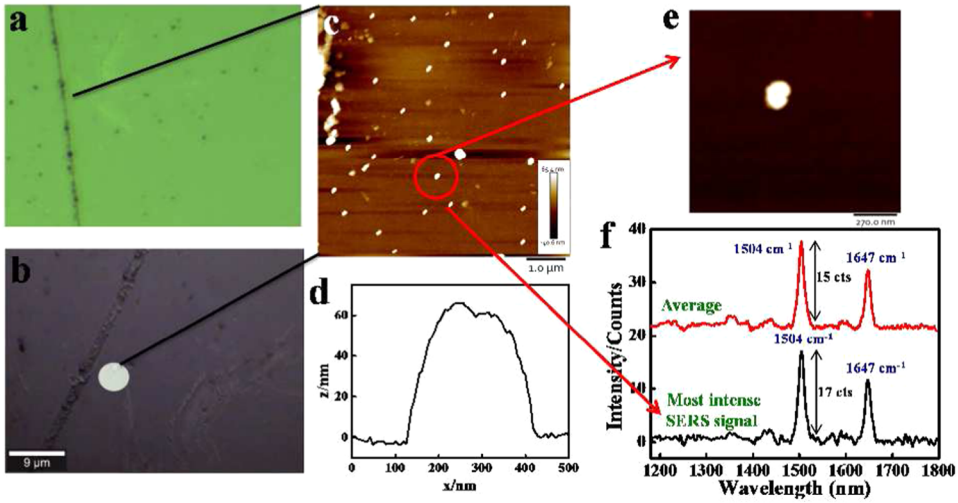

Figure 7. AFM-correlated Raman measurements using 633 nm laser source. (a) Optical image taken using 10× objective of AFM. (b) Optical image taken using 100× objective of confocal Raman microscope. (c) AFM images of Au nanostar dimer with gap of 7 nm and (d) corresponding height profile. (e) AFM image of single Au nanostar dimer nanostructure.(f) Average and most intense SERS spectra of TR dye bound to bound to Au nanostar dimer on DNA origami.

used in single-molecule SERS measurement using two different laser sources of 532 and 633 nm wavelength. In this study, a single TR dye molecule which is placed specifically inside DNA origami in between two Au nanostars acts as a Raman reporter moiety. AFM correlated Raman measurements were performed by scanning almost the same area by AFM imaging and confocal Raman microscopy. At first, images taken by optical microscope of AFM and confocal Raman microscope as shown in Figures 6a,b and 7a,b were overlapped by identification of pronounced features in images with precise accuracy. This was followed by scanning that particular area by AFM (Figures 6c and 7c) and then doing Raman measurements of the same area. Figures 6d and 7d represent the height profile of the recorded AFM images shown in Figures 6c and 7c which confirm the presence of Au nanostar dimer structures on origami. Figures 6e and 7e are the AFM images of single Au nanostar dimer nanostructures. The average and most intense AFM correlated SERS spectra of TR dye bound to Au nanostar dimer on DNA origami with nanogap of 7 nm using laser excitation wavelengths of 532 and 633 nm are shown in Figures 6f and 7f, respectively. Here, the Raman spectra were collected in the 1100−1800 cm^{-1} region, and the samples were scanned with a laser power of 1 mW. We recorded Raman spectra of TR dye bound to nanostar dimers at different positions of the selected area and calculated the mean enhancement factor. From the Raman spectra acquired at different regions of selected area it was found that peak intensity remains almost same (Figures 6f and 7f). For calculating SERS EF, I_{SERS} was taken from the strongest Raman peaks of the TR dye, which are 1647 and 1504 cm^{-1} for 532 and 633 nm laser excitation, respectively.[24,50] Mean enhancement factor was calculated by taking ∼25 different spectra acquired from 25 different structures of selected area. Overlaid single-molecule Raman spectra of TR dye from 12 different Au nanostar dimer nanostructures (nanogap ∼7 nm with 633 nm laser excitation) and corresponding AFM images are shown in Figure S3. The mean enhancement factor has been calculated based on the average Raman band intensity of TR bound to Au nanostar dimer after comparing with Raman band of TR bulk (1.5 mM) solution on Si surface. It has been observed from the AFM images of Au nanostar dimers that only one nanostructure is present in the spatial focal area (shown in the circles of Figures 6c and 7c). The corresponding Raman spectra of a single TR dye bound to Au nanostar dimer are shown in Figures 6f and 7f with different laser excitation. A reference Raman spectrum of TR dye (shown in Figure S4) was obtained by casting the TR solution (0.5 μM) on the surface of 50 nm spherical Au nanoparticles uniformly distributed over Si substrate with 532 and 632 nm laser sources. It can be seen that, in the single-molecule regime, spectral stability is lost due to the loss of ensemble averaging.

To analyze the level of background contribution and the suitability of DNA origami-based SERS substrates we performed control experiments by measuring Raman spectra of samples comprising Au nanostars, Au nanostar dimer on DNA origami, and DNA origami without any TR dye. All control experiments were done by using both 532 and 633 nm laser excitation sources. To avoid melting of DNA origami nanostructures because of heat generated upon using high laser power, for single-molecule experiments laser power was set to 1 mW. No Raman peaks were obtained for Au nanostars only (Figure 8a,c) and DNA origami without any TR dye (Figure 8b,d). The Raman spectrum of Au nanostar dimer on DNA origami without any TR dye showed no peak with both 532 and 633 nm laser source in almost all the Raman spectra (inset of Figure 8a,c). However, when measurement was done with much higher laser power (∼1.8 mW) two new peaks appeared as represented in Figure S5. The peaks observed at 1331 and 1568 cm^{-1} can be ascribed to DNA surrounding the Au nanostars[30] and were originated due to the electromagnetic field enhancement generated by the sharp tips of Au nanostars providing SERS enhancement for the DNA located in the hotspot.[30] It is interesting to note that no Raman signals correspond to TR dye were observed for TR dye bound to DNA origami in absence of Au nanostar even with a high laser power of 1 mW for both 532 and 633 nm laser excitation (inset of Figure 8b,d). Raman spectra of TR dye bound to Au nanostar dimers on DNA origami with different nanogaps are shown in Figure 9. Two main Raman peaks were obtained at 1501 and 1647 cm^{-1} which correspond to TR dye and intensity

DOI: 10.1021/jacs.7b10410
J. Am. Chem. Soc. 2017, 139, 17639−17648

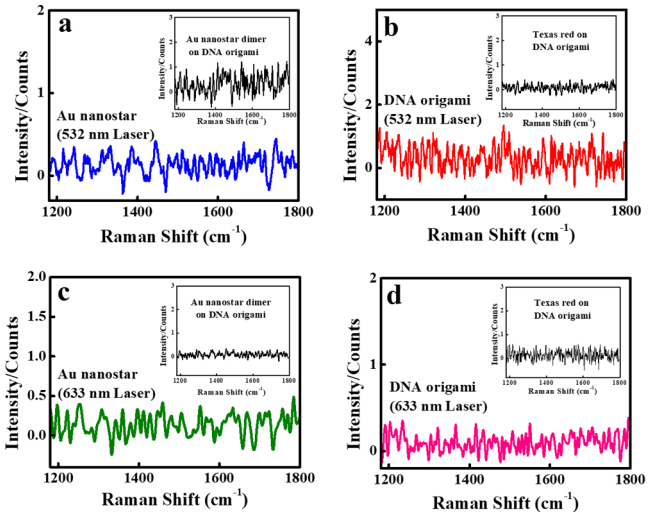

Figure 8. Raman spectra of (a) Au nanostar using 532 nm laser source (Au nanostar dimer on DNA origami without TR dye is shown in inset profile); (b) DNA origami using 532 nm laser source (TR dye on DNA origami without Au nanostar is shown in inset profile); (c) Au nanostar using 633 nm laser source (Au nanostar dimer on DNA origami without TR dye is shown in inset profile); and (d) DNA origami using 633 nm laser source (TR dye on DNA origami without Au nanostar is shown in inset profile).

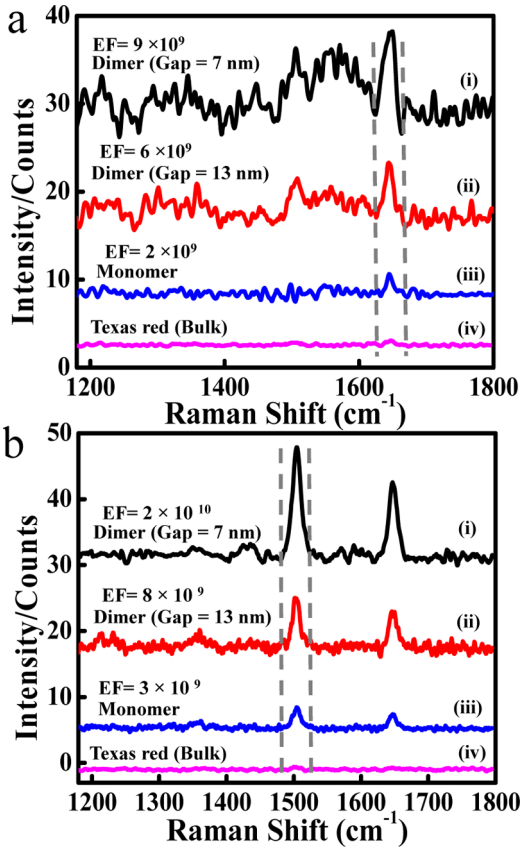

Figure 9. (a) SERS spectra of TR dye bound to Au nanostar dimers with average gaps of 7 nm (curve (i)) and 13 nm (curve (ii)), and TR dye bound to Au nanostar monomer on DNA origami (curve (iii)) and bulk TR dye (curve (iv)) recorded using 532 nm laser. (b) SERS spectra of TR dye bound to Au nanostar dimers with average gaps of 7 nm (curve (i)) and 13 nm (curve (ii)), and TR dye bound to Au nanostar monomer on DNA origami (curve (iii)) and bulk TR dye (curve (iv)) recorded using 633 nm laser.

of these peaks were slightly decreased upon increasing the interparticle distance from 7 to 13 nm. Further, we have investigated the Raman spectrum of the TR dye bound to Au nanostar monomer on dimerized DNA origami as presented in Figure 9. Intensities of various peaks were almost halved from Au nanostar dimer to monomer due to the absence of plasmon coupling in monomer providing less SERS enhancement of TR dye for monomer. Single TR molecules placed in between two Au nanostars of nanostar dimers experience an enhanced electric field, leading to an increase in the intensity of the Raman signal compared to nanostar monomer, which is in consistent with previous result.[24,57] The mean enhancement factors of TR dye were found to be 9×10^9 and 6×10^9 using 532 nm laser excitation and 2×10^{10} and 8×10^9 using 633 nm laser excitation for Au nanostar dimers with gaps of 7 and 13 nm, respectively (shown in Table 1), which are sufficient enough for single TR molecule detection.[28] For TR dye bound to Au nanostar monomer, calculated averaged EF is 2×10^9 when 532 nm laser used. In SERS enhancement factor calculation error can result from different molecular orientation. We have estimated the error in mean EFs calculation by taking intensity of characteristic Raman peaks of different SERS spectra and was found to be ∼17%. It is clearly seen in the present study that the magnitude of electromagnetic field enhancement in the conjunction region decreases with increasing interparticle distance of nanostar dimer, revealing less SERS enhancement for both the lasers used. The order of distance dependence of EF was found to be in good agreement with previous results.[24,58] The mean EF of TR is increased by a factor of ∼4 in case of 532 nm laser and by a factor of ∼5 in case of 633 nm laser from monomer nanostar to dimer nanostar (gap = 7 nm). This agrees very well with the experimentally observed variation of the peak intensities (at 1647 and 1504 cm^{-1}) between SERS of TR bound to Au nanostar dimer on origami and nanostar monomer on origami structures as shown in Figure 9. Further, calculated EFs were found to be higher for 633 nm laser than 532 nm laser by a factor of ∼2. Higher value of EF for 633 nm laser can be attributed due to close resonance between wavelength of laser source and LSPR of Au nanostars. It is well reported that mean EF of Raman reporters increases from monomer to dimer due to the presence of hotspot in the dimeric junction. Ma et al. showed the similar trend of SERS intensity enhancement of 4-ATP in Au nanostar dimer structures compared to single nanostar,[57] which agrees very well with our findings. It has been very recently demonstrated by Bukasov et al. that the EF increases upon dimerization by 1−2 orders of magnitude relative to the mean EF of single NPs.[59]

The ratio of the mean intensity or mean EF of dimers to the mean intensity or mean EF of monomers (I_d/I_m or EF_d/EF_m) for NPs on substrates depends on the nature of NPs, substrates and the position of the LSPR frequencies relative to the frequency of the exciting laser.[59] They have observed that the mean EF of 2-ATP molecule measured on Si surface was increased by a factor of 4.8 when placed in the hotspot of 60 nm sized Au NPs dimer to single Au NP whereas the mean EF ratios were 1.61 and 1.42 for Ag and Au surfaces, respectively. Our experimental findings yield the increase of mean EF of TR dye measured on Si surface by a factor of ∼5 from monomer nanostar to dimer nanostar (gap = 7 nm) which corroborates the results reported by Bukasov et al. Furthermore, it has been

DOI: 10.1021/jacs.7b10410
J. Am. Chem. Soc. 2017, 139, 17639−17648

Table 1. Experimentally Obtained Data from SERS Measurements

system	average interparticle gap, nm	Raman peak intensity of TR dye (1647 cm^{-1})	mean enhancement factor (532 nm laser)	Raman peak intensity of TR dye (1504 cm^{-1})	mean enhancement factor (633 nm laser)
Au nanostar monomer	–	2.4	2×10^9	3.2	3×10^9
Au nanostar dimer	13	6.43	6×10^9	7.7	8×10^9
Au nanostar dimer	7	9.86	9×10^9	17	2×10^{10}

reported that by changing the negative curvature site of metal nanostructure, the plasmon coupling and the local field enhancement can be controlled.[60] The negative curvature of the nanostars can be changed either by changing metal core size or by changing the no of branches of the stars. In the present study, we have increased the negative curvature regions of Au nanostars by decreasing the number of branches of the nanostars to study its influence on the SERS responses of the nanostar dimer structures. We have measured the SERS activities of Au nanostar dimers (7 nm nanogap as shown in Figure S6a) with nanostar having lesser number of tips (radius of curvature of tips ∼4−6 nm, number of branches ∼6−7) and the corresponding SERS spectrum is shown in Figure S6. It was found that the EF decreases by a factor of ∼13 for nanostar dimer structures with higher negative curvature. This is due to the increase of separation distance between tips in the nanostar which can decrease the coupling between the tips and minimize the local field enhancement as mentioned by Odom et al.[46] for Au nanocrescent type of structures.

In an attempt to identify the total number of TR molecules contributing in the SERS signal, we considered the laser focal area of 1 μm^2.[21] After careful examination of the AFM images (shown in Figures 6c and 7c), we have found that only one Au nanostar dimer (assembled on DNA origami) structure is resided in the laser focal area. Now each origami structure (Au NS dimer) contains a single TR dye specifically bound in the origami, so there will be one dye present in the focal spot, and hence one independent single TR molecule is contributing in the Raman signal. The strongest Raman bands of TR dye, located at 1647 and 1504 cm^{-1}, are clearly visible in the SERS spectra of TR for both monomer and dimer nanostars and become even more pronounced for dimer nanostar. At lower interparticle gap (7 nm), the signal increases prominently due to much stronger plasmon coupling between sharp tips and cores of two Au nanostars in the wide conjunction region. Our experimental findings confirms that the SERS-based detection of single TR molecule is possible after placing the dye in the center of the conjunction region of Au nanostar dimer bound to DNA origami structure. Moreover, in a remarkable observation, it was noted that the highly enhanced electromagnetic field generated by the coupling of sharp tips of Au nanostars exhibits excellent SERS sensitivity even at an interparticle separation distance of 13 nm. Thus, the Au nanostar dimeric structures on origami have highly SERS-active wide conjunction region that can provide enough space for the accommodation of large biomolecule of interest (such as protein) to enable its specific detection via single-molecule SERS.

CONCLUSIONS

In summary, we have demonstrated the synthesis of Au nanostar dimer with tunable interparticle gap and controlled stoichiometry assembled on rectangular DNA origami. DNA origami technique provides a reliable fabrication method to build probes of strongly coupled nanostructure dimers with precisely controlled particle spacing with sub nm accuracy, spatial orientation and well-defined geometry in order to create plasmonic hotspots of tunable strength. SERS measurements of single TR dye molecule which is specifically placed in the center of dimerized origami from such Au nanostar−DNA origami hybrid structures with different nanogaps have been presented. We have shown that the most intense Raman bands of TR dye can be clearly identified in the SERS spectra of single TR dye molecules in both monomer and dimer nanostars on DNA origami substrates. The mean EFs of TR dye were obtained to be in the order of 10^{10}, which are high enough for single-analyte detection. Consequently, the detection of single analyte molecules with much lower Raman cross sections might be feasible by using these structures. Such hybrid nanoantennas assembled on DNA origami with controlled interparticle distance and stoichiometry act as excellent SERS substrates and will have potential applications as a cost-effective and reproducible platform for single-molecule sensing. Importantly, DNA origami offers several sequence-specific binding sites where a wide variety of biomolecules can be attached specifically at the hotspot region with great precision, and this may allow molecules to be targeted at a single-molecule level.

ASSOCIATED CONTENT

Supporting Information

The Supporting Information is available free of charge on the ACS Publications website at DOI: 10.1021/jacs.7b10410.

Figure S1, PL spectra of Texas red dye in DNA origami; Figure S2, TEM images of Au nanostar on DNA origami with touching tips and corresponding Raman spectrum; Figure S3, AFM images of 12 different Au nanostar dimer nanostructures (7 nm nanogap) and corresponding single-molecule SERS spectra acquired using 633 nm laser excitation; Figure S4, structure of TR dye and reference Raman spectrum using 532 and 633 nm laser excitation; Figure S5, Raman spectrum of Au nanostar dimer on DNA origami; Figure S6, TEM images of Au nanostar dimer (nanogap ∼7 nm) and corresponding single-molecule SERS spectrum of TR dye in plasmonic hotspot; Scheme S1, dimerized rectangular DNA origami design for synthesis of Au nanostar dimer with interparticle gap; Table S1, DNA origami staple sequences; Tables S2 and S3, edge staple sequences; Tables S4 and S5, branching staple sequences; Table S6, dye-labeled sequence; and Table S7, thiol-labeled sequence (PDF)

DOI: 10.1021/jacs.7b10410
J. Am. Chem. Soc. 2017, 139, 17639−17648

AUTHOR INFORMATION

Corresponding Author

*tapasi@inst.ac.in

ORCID

Krishna Kanta Haldar: 0000-0002-0675-8299

Tapasi Sen: 0000-0003-0243-178X

Notes

The authors declare no competing financial interest.

ACKNOWLEDGMENTS

T.S. thanks Department of Science and Technology (DST, SERB Project ECR/2016/000436) for financial support and INST for instrumental facility and infrastructural support. S.T. gratefully acknowledges INST for the Ph.D. fellowship. Ashok K. Ganguli is gratefully acknowledged for stimulating discussion.

REFERENCES

(1) Rothemund, P. W. *Nature* **2006**, *440*, 297.
(2) Rajendran, A.; Endo, M.; Sugiyama, H. *Angew. Chem., Int. Ed.* **2012**, *51*, 874.
(3) Samanta, A.; Zhou, Y.; Zou, S.; Yan, H.; Liu, Y. *Nano Lett.* **2014**, *14*, 5052.
(4) Acuna, G. P.; Bucher, M.; Stein, I. H.; Steinhauer, C.; Kuzyk, A.; Holzmeister, P.; Schreiber, R.; Moroz, A.; Stefani, F. D.; Liedl, T.; Simmel, F. C.; Tinnefeld, P. *ACS Nano* **2012**, *6*, 3189.
(5) Acuna, G. P.; Möller, F. M.; Holzmeister, P.; Beater, S.; Lalkens, B.; Tinnefeld, P. *Science* **2012**, *338*, 506.
(6) Thacker, V. V.; Herrmann, L. O.; Sigle, D. O.; Zhang, T.; Liedl, T.; Baumberg, J. J.; Keyser, U. F. *Nat. Commun.* **2014**, *5*, 3448.
(7) Simoncelli, S.; Roller, E. M.; Urban, P.; Schreiber, R.; Turberfield, A. J.; Liedl, T.; Lohmuller, T. *ACS Nano* **2016**, *10*, 9809.
(8) Rodríguez-Lorenzo, L.; Álvarez-Puebla, R. A.; Pastoriza-Santos, I.; Mazzucco, S.; Stéphan, O.; Kociak, M.; Liz-Marzán, L. M.; García de Abajo, F. J. *J. Am. Chem. Soc.* **2009**, *131*, 4616.
(9) Bell, S. E. J.; Sirimuthu, N. M. S. *J. Am. Chem. Soc.* **2006**, *128*, 15580.
(10) Chou, A.; Jaatinen, E.; Buividas, R.; Seniutinas, G.; Juodkazis, S.; Izake, E. L.; Fredericks, P. M. *Nanoscale* **2012**, *4*, 7419.
(11) Cheng, H. W.; Huan, S. Y.; Wu, H. L.; Shen, G. L.; Yu, R. Q. *Anal. Chem.* **2009**, *81*, 9902.
(12) Cao, Y. W. C.; Jin, R. C.; Mirkin, C. A. *Science* **2002**, *297*, 1536.
(13) Aizpurua, J.; Bryant, G. W.; Richter, L. J.; de Abajo, F. J. G.; Kelley, B. K.; Mallouk, T. *Phys. Rev. B: Condens. Matter Mater. Phys.* **2005**, *71*, 235420.
(14) Brown, L. V.; Yang, X.; Zhao, K.; Zheng, B. Y.; Nordlander, P.; Halas, N. J. *Nano Lett.* **2015**, *15*, 1272.
(15) Cetin, A. E.; Etezadi, D.; Altug, H. *Adv. Opt. Mater.* **2014**, *2*, 866.
(16) Sen, T.; Patra, A. *J. Phys. Chem. C* **2012**, *116*, 17307.
(17) Novotny, L.; van Hulst, N. *Nat. Photonics* **2011**, *5*, 83.
(18) Suh, J. Y.; Odom, T. W. *Nano Today* **2013**, *8*, 469.
(19) Sen, T.; Mandal, S.; Haldar, S.; Chattopadhyay, K.; Patra, A. *J. Phys. Chem. C* **2011**, *115*, 24037.
(20) Kuhler, P.; Roller, E. M.; Schreiber, R.; Liedl, T.; Lohmuller, T.; Feldmann, J. *Nano Lett.* **2014**, *14*, 2914.
(21) Prinz, J.; Heck, C.; Ellerik, L.; Merk, V.; Bald, I. *Nanoscale* **2016**, *8*, 5612.
(22) Greeneltch, N. G.; Blaber, M. G.; Henry, A. I.; Schatz, G. C.; Van Duyne, R. P. *Anal. Chem.* **2013**, *85*, 2297.
(23) Barbosa, S.; Agrawal, A.; Rodriguez-Lorenzo, L.; Pastoriza-Santos, I.; Alvarez-Puebla, R. A.; Kornowski, A.; Weller, H.; Liz-Marzan, L. M. *Langmuir* **2010**, *26*, 14943.
(24) Kumar, J.; Thomas, K. G. *J. Phys. Chem. Lett.* **2011**, *2*, 610.
(25) Harmsen, S.; Bedics, M. A.; Wall, M. A.; Huang, R.; Detty, M. R.; Kircher, M. F. *Nat. Commun.* **2015**, *6*, 6570.
(26) Fales, A. M.; Yuan, H.; Vo-Dinh, T. *J. Phys. Chem. C* **2014**, *118*, 3708.
(27) Esenturk, E. N.; Walker, A. R. H. *J. Raman Spectrosc.* **2009**, *40*, 86.
(28) Lim, D.-K.; Jeon, K.-S.; Kim, H. M.; Nam, J.-M.; Suh, Y. D. *Nat. Mater.* **2010**, *9*, 60.
(29) Nie, S.; Emory, S. R. *Science* **1997**, *275*, 1102.
(30) Prinz, J.; Schreiber, B.; Olejko, L.; Oertel, J.; Rackwitz, J.; Keller, A.; Bald, I. *J. Phys. Chem. Lett.* **2013**, *4*, 4140.
(31) Heck, C.; Prinz, J.; Dathe, A.; Merk, V.; Stranik, O.; Fritzsche, W.; Kneipp, J.; Bald, I. *ACS Photonics* **2017**, *4*, 1123.
(32) Prinz, J.; Matković, A.; Pešić, J.; Gajić, R.; Bald, I. *Small* **2016**, *12*, 5458.
(33) Khoury, C. G.; Vo-Dinh, T. *J. Phys. Chem. C* **2008**, *112*, 18849.
(34) Shiohara, A.; Langer, J.; Polavarapu, L.; Liz-Marzan, L. M. *Nanoscale* **2014**, *6*, 9817.
(35) Barbosa, S.; Topete, A.; Alatorre-Meda, M.; Villar-Alvarez, E. M.; Pardo, A.; Alvarez-Lorenzo, C.; Concheiro, A.; Taboada, P.; Mosquera, V. *J. Phys. Chem. C* **2014**, *118*, 26313.
(36) Rodriguez-Lorenzo, L.; de la Rica, R.; Alvarez-Puebla, R. A.; Liz-Marzan, L. M.; Stevens, M. M. *Nat. Mater.* **2012**, *11*, 604.
(37) Huang, Y.; Duan, X. F.; Wei, Q. Q.; Lieber, C. M. *Science* **2001**, *291*, 630.
(38) Nehl, C. L.; Liao, H. W.; Hafner, J. H. *Nano Lett.* **2006**, *6*, 683.
(39) Punj, D.; Regmi, R.; Devilez, A.; Plauchu, R.; Moparthi, S. B.; Stout, B.; Bonod, N.; Rigneault, H.; Wenger, J. *ACS Photonics* **2015**, *2*, 1099.
(40) Kinkhabwala, A.; Yu, Z.; Fan, S.; Avlasevich, Y.; Mullen, K.; Moerner, W. E. *Nat. Photonics* **2009**, *3*, 654.
(41) Stranik, O.; Nooney, R.; McDonagh, C.; MacCraith, B. D. *Plasmonics* **2007**, *2*, 15.
(42) Rodríguez-Lorenzo, L.; Álvarez-Puebla, R. A.; de Abajo, F. J. G.; Liz-Marzán, L. M. *J. Phys. Chem. C* **2010**, *114*, 7336.
(43) Lu, G.; Forbes, T. Z.; Haes, A. J. *Analyst* **2016**, *141*, 5137.
(44) Solís, D. M.; Taboada, J. M.; Obelleiro, F.; Liz-Marzán, L. M.; García de Abajo, F. J. *ACS Photonics* **2017**, *4*, 329.
(45) Esteban, R.; Zugarramurdi, A.; Zhang, P.; Nordlander, P.; Garcia-Vidal, F. J.; Borisov, A. G.; Aizpurua, J. *Faraday Discuss.* **2015**, *178*, 151.
(46) Odom, T. W.; You, E.-A.; Sweeney, C. M. *J. Phys. Chem. Lett.* **2012**, *3*, 2611.
(47) Indrasekara, A. S. D. S.; Meyers, S.; Shubeita, S.; Feldman, L. C.; Gustafsson, T.; Fabris, L. *Nanoscale* **2014**, *6*, 8891.
(48) Liber, M.; Tomov, T. E.; Tsukanov, R.; Berger, Y.; Nir, E. *Small* **2015**, *11*, 568.
(49) Jungmann, R.; Scheible, M.; Kuzyk, A.; Pardatscher, G.; Castro, C. E.; Simmel, F. C. *Nanotechnology* **2011**, *22*, 275301.
(50) Moula, G.; Aroca, R. F. *Anal. Chem.* **2011**, *83*, 284.
(51) Liu, R.; Hu, D.; Tan, X.; Lu, H. P. *J. Am. Chem. Soc.* **2006**, *128*, 10034.
(52) Yuan, H.; Khoury, C. G.; Hwang, H.; Wilson, C. M.; Grant, G. A.; Vo-Dinh, T. *Nanotechnology* **2012**, *23*, 075102.
(53) Turkevich, J.; Stevenson, P. C.; Hillier, J. *Discuss. Faraday Soc.* **1951**, *11*, 55.
(54) Mirkin, C. A.; Letsinger, R. L.; Mucic, R. C.; Storhoff, J. J. *Nature* **1996**, *382*, 607.
(55) Jana, D.; Mandal, A.; De, G. *ACS Appl. Mater. Interfaces* **2012**, *4*, 3330.
(56) Paital, D.; Sen, T.; Patra, A.; Haldar, K. K. *Gold Bull.* **2017**, DOI: 10.1007/s13404-017-0220-1.
(57) Ma, W.; Sun, M. Z.; Xu, L. G.; Wang, L. B.; Kuang, H.; Xu, C. L. *Chem. Commun.* **2013**, *49*, 4989.
(58) Shanthil, M.; Thomas, R.; Swathi, R. S.; George Thomas, K. *J. Phys. Chem. Lett.* **2012**, *3*, 1459.
(59) Sergiienko, S.; Moor, K.; Gudun, K.; Yelemessova, Z.; Bukasov, R. *Phys. Chem. Chem. Phys.* **2017**, *19*, 4478.
(60) Zhu, J.; Ren, Y.-j. *J. Nanopart. Res.* **2012**, *14*, 1326.

DOI: 10.1021/jacs.7b10410
J. Am. Chem. Soc. 2017, 139, 17639−17648